JOURNAL OF PHYSICAL ORGANIC CHEMISTRY
J. Phys. Org. Chem. 2000; **13:** 489–498

Regio- and stereoselectivity of [2 + 3] cycloaddition of (*E*)-*β*-nitrostyrenes to (*Z*)-C,N-diphenylnitrone in the light of AM1 and AM1/COSMO calculations†

Andrzej Baranski,* Marta Olszanska and Katarzyna Baranska

Department of Organic Chemistry, Krakow Technical University, 31–155 Krakow, Poland

Received 21 November 1999; revised 10 February 2000; accepted 22 March 2000

ABSTRACT: Four isomeric pathways for the [2 + 3] cycloaddition of (*E*)-*β*-nitrostyrenes (**1a**–**c**) with (*Z*)-C,N-diphenylnitrone (**2**) in gas phase and in a dielectric medium corresponding to the relative permittivity of toluene was evaluated in terms of AM1 and AM1/COSMO calculations in order to predict the reaction regio- and stereoselectivity. It was found that in the gas phase reaction takes place in a concerted manner independent of the nitrostyrene used as a dipolarophile and the [2 + 3] cycloadduct formed. The activation barriers obtained indicate that paths **B** and **D** (Scheme 1) are favored. The highest activation barrier occurs on the path **C**. In toluene solution this trend changes and the reaction paths can be ordered in the sequence **B** > **A** > **D** > **C**. An increase in the polarity of the reaction medium elevates the activation barriers and in some cases changes the reaction mechanism. An increase in the electron-withdrawing character of the substituent in the benzene ring of (*E*)-*β*-nitrostyrene speeds up the reaction both in the gas phase and in toluene solution but does not affect the reaction regio- and stereoselectivity. Copyright © 2000 John Wiley & Sons, Ltd.

KEYWORDS: AM1 calculations; COSMO; hypersurface; [2 + 3] cycloaddition; nitroalkenes; nitrones

INTRODUCTION

The present paper is intended as a continuation of our studies concerning the reactivity of conjugated nitroalkenes in [2 + 3] cycloaddition reactions.[1–3] In particular, its goal was to evaluate the substituent effect in nitroalkene on the regio and stereoselectivity of the reaction between (*E*)-*β*-nitrostyrenes (**1a**–**c**) and (*Z*)-C,N-diphenylnitrone (**2**) (Scheme 1). The [2 + 3] cycloadditions are the core of the pericyclic reactions and an understanding of structure-reactivity correlation in these processes is essential from both theoretical and practical point of view.

It is generally accepted[4–6] that alkene–nitrone cycloadditions can occur with the alkene and nitrone approaching each other in either of two possible regiochemical manners and in either an *endo* or *exo* fashion giving rise to two pairs of regio- and stereoisomeric products. In the case of reactants studied the expected products should be 2,3-diphenyl-5-aryl-4-nitroisoxazolidines (**3a**–**c**, **4a**–**c**) and 2,3-diphenyl-4-aryl-5-nitroisoxazolidines (**5a**–**c**, **6a**–**c**). However, at 353 K in toluene solution, a high degree of regiocontrol was observed and 4-nitroisoxazolidines (**3a**–**c** and **4a**–**c**) were obtained as the only reaction products.[7–9]

In order to gain a better insight into the regio- and stereochemical aspects of the reaction, quantum chemical studies of the competitive paths **A**–**D** in the gas phase and in a dielectric medium corresponding to the relative permittivity of toluene were carried out. For each of them

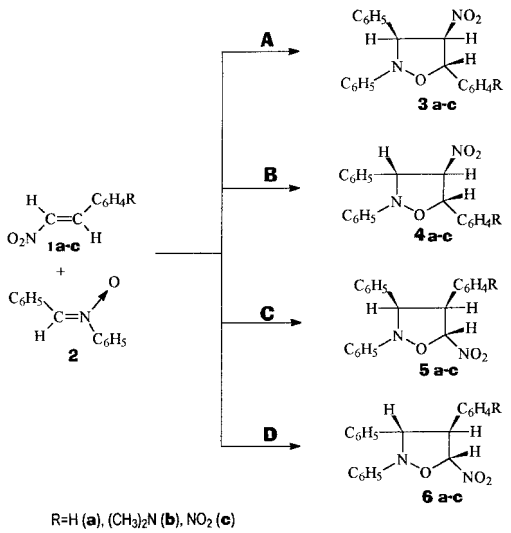

Scheme 1

**Correspondence to:* A. Baranski, Department of Organic Chemistry, Cracow Technical University, 31–155 Krakow, Poland.
† Part XLIV in the series Synthesis and Properties of Azoles and Their Derivatives. Part XLIII: *Polish J. Chem.* 1999; **73:** 1711.
Contract/grant sponsor: Polish Committee of Scientific Research; *Contract/grant number:* KBN/SPP/PK/076.

Table 1. Selected physical and structural parameters for (*E*)-*β*-nitrostyrene (**1a**) and (*Z*)-C,N-diphenylnitrone (**2**) as calculated by the three semiempirical methods and observed by experiment

	1a			**2**				
Method	I (eV)	μ(D)	$I_{C=C}$ (Å)	I (eV)	μ[D]	$I_{C=N}$ (Å)	$I_{N—O}$ (Å)	$\angle_{O—N=C}$ (°)
MNDO	9.73	6.12	1.354	8.81	4.05	1.347	1.228	125.02
AM1	9.89	6.06	1.347	8.40	3.78	1.337	1.228	126.14
PM3	10.04	6.08	1.345	8.66	4.17	1.336	1.242	127.78
Experiment	9.12 [19]	4.51 [20]	—	7.40 [21]	3.44 [22]	1.297 [23]	1.289 [23]	124.40 [23]

the activation parameters were determined. Although [2 + 3] cycloaddition of conjugated nitroalkenes to nitrones is a widely used method for the preparation of nitroisoxazolidines,[10,11] these reactions were not the object of theoretical studies in the past. As far as we know, only [2 + 3] cycloaddition of nitroethylene to the parent nitrone was explored by means of the AM1 method by Pascal *et al.*[12] and the regioselectivity of the process was evaluated in good agreement with experimental data.

CALCULATION PROCEDURE

The calculations were performed on the CONVEX SPP 1600/XA computer at the regional computer center CYFRONET in Krakow, using the MOPAC-93 program package.[13] Considering the number and size of the molecular systems that are the subject of the present study, the choice of a semiempirical method was necessary. Because some experimental data are available for **1a** and **2**, these compounds were used to select the most appropriate method among MNDO, AM1 and PM3 for our calculations. As can be seen from Table 1, the AM1 model leads to the closest agreement with the observed parameters and therefore this method was adopted for all further calculations.

For the purpose of the reaction path simulation, the substrates were placed 12.5 Å apart and the geometry for the so-obtained supermolecule (**R**) was optimized with the EF procedure. This geometry was used in combination with the final [2 + 3] cycloadduct geometry (**P**) to localize the saddle point for each possible reaction path by means of the SADDLE routine. The transition-state structures (**TS**) were subsequently optimized with NLLSQ and TS procedures and their nature were confirmed by calculations of the Hessian matrix and by intrinsic reaction coordinate (IRC) calculations. The calculations indicated that all **TS** structures showed only one negative force constant, while IRC calculations provided structures associated with the local minimuma (**LM**) and cycloadducts (**P**).

The COSMO algorithm of Klamt and Schüürmann,[14] as implemented in the MOPAC 93 program package, was applied to the solvent simulation. In this method, the solvent is taken into account by means of its dielectric constant (EPS), effective solvation radius (RSOLV), and the parameter which defines the solvent accessible surface area (NSPA). It was assumed that EPS = 2.4 and NSPA = 40. Following the recommendations of the authors of the method,[14] it was assumed that RSOLV = 1. The same Hamiltonian and the same calculation methodology were applied to the toluene solution as to the gas phase. However, a major problem was detected with MOPAC-93 in that all IRC calculations failed to complete correctly when the COSMO procedure was used. Therefore, **TS** structures were in turn verified by increasing and decreasing the lengths of the newly formed *σ*-bonds by 0.02 Å, and optimizing the so-obtained geometry with the EF procedure. In this way minima associated with **LM, P** and intermediate **I** structures were localized.

All stationary structures were optimized to a gradient norm of less than 0.2 in the gas phase and 0.4–0.6 in toluene solution. The absolute entropies of all structures were calculated from a complete vibrational analysis. Enthalpies were corrected to the free energies using calculated entropies. The calculations presented in this paper were carried out for 353 K.

RESULTS AND DISCUSSION

The AM1 calculations indicated that irrespective of the pair of reactants used, for each gas-phase reaction

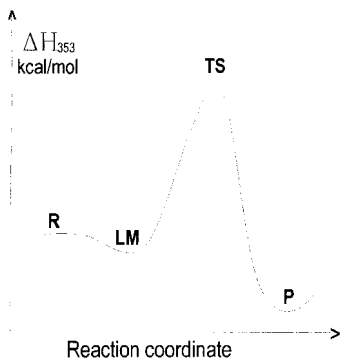

Figure 1. Typical reaction profile for the [2 + 3] cycloaddition of (*E*)-*β*-nitrostyrenes **1a**–**c** with (*Z*)-C, N-diphenylnitrone **2** in the gas phase. Structures at the marked points are depicted in Fig. 2

pathway between the structures of the reactants **R** and final products **P** studied two stationary structures can be localized (Fig. 1).

The values of the heats of formation (ΔH_{353}), entropies ΔS_{353}), dipole moments (η), charge transfer (t) and charges on the reaction sites (d) and some essential geometric dimensions are shown in Table 2. The magnitude of charge transfer in the critical structures was obtained by Mulliken population analysis using an expression given by Leroy *et al.*[15] The positive value of the charge transfer denotes the charge shift from the substructure of 1,3-dipole to the one of dipolarophile. Figure 2 shows PLUTO views of critical structures associated with substrates **1a** and **2**. The critical structures associated with the other reactants were similar to those shown. The values of relative thermodynamic parameters of the local minimas, transition states and products are presented in Table 3.

Initially, as can be seen from Fig. 1, interaction of nitrostyrenes **1a–c** with nitrone **2** in the gas phase leads without an activation barrier to a suitable **LM** on the potential energy hypersurface (PES). During this transition, the geometry of the reactants remains practically intact; the substrates only rearrange in space so as to provide the most favorable electrostatic interaction. No charge transfer was observed in any of the substrate arrangements corresponding to particular **LM**. These arrangements resulted from IRC calculations of the individual reaction paths, but **LM** structures indicate that they are not directly related to the $[2+3]$ cycloaddition process. They result rather from the tendency of the system for energy minimization. In such huge systems with many degrees of freedom, there are many local minima on the PES. Which of the minima is found by the IRC procedure depends only on the assumed initial conditions. Indeed, within the structures found for the local minima, there is no apparent relationship between the substrate arrangements and the nature of substituent in (*E*)-*β*-nitrostyrene or the type of isoxazolidine isomer formed. Hence, the **LM** structures can be treated as the minima on the PES only in respect of their enthalpy of formation, while the magnitude of $\Delta H^{\neq}_{353}$may vary between -2.5 and -7.4 kcal mol^{-1} (1 kcal = 4.184 KJ) depending on the type of nitrostyrene and the reaction path. However, from the thermodynamic point of view, $\Delta G^{\neq}_{353}$values exclude the existence of stable **LM** structures at ambient or elevated temperatures, because of large negative entropy changes associated with the formation of these structures in each of the analyzed reactions. It should be noted that the IRC calculations give the reaction path of minimal energy at 298 K. The difference in the $\Delta H°_f$ of **LM** and **R** structures is equal to the difference in SCF energies for AM1. The FORCE and THERMO procedures allow adding translational, rotational and vibrational contributions at 353 K from classical statistical mechanical formula. These formula come, however, from partition functions, which do not correspond to a total sampling of the PES, and therefore the ΔS values can be impaired by a relatively large error.[13]

The motion forward along the reaction paths **A–D** towards cycloadducts **P** leads to transition states **TS**. Within these structures (Fig. 2), the substituents attached to the C═C double bond of dipolarophile and C═N double bond of 1,3-dipole are deflected away from the reaction site, because of rehybridization of the atoms at the site. The substituents reorient themselves so as to assume the position they occupy in the final product. Although these structures suggest a concerted reaction mechanism, they are not fully symmetric. The new σ-bonds are formed simultaneously but not to the same extent, as indicated by values of the C5—O1 and C3—C4 bond length (Table 2). In the case of the studied reaction paths, independently of the substrate pair selected, the C5—O1 bond is formed faster than the C3—C4 bond, but the transition states involved in paths **C** and **D** are significantly more symmetric. This phenomenon can be explained in terms of charge distribution within the substructures in **LM** complexes. In the substructure of diphenylnitrone **2** there is a large negative charge localized on the oxygen atom. In (*E*)-*β*-nitrostyrenes **1a–c** there is a large negative charge on the carbon atom adjacent to the nitro group and a very small charge on the carbon atom adjacent to the aryl ring. This causes stronger repulsion between the corresponding carbon and oxygen atoms when 5-nitroisoxazolidines **5a–c** and **6a–c** are formed compared with the formation of the 4-nitroisoxazolines **3a–c** and **4a–c**.

The Mulliken population analysis of charge distribution within the transition states indicates that the charge shift occurs from the substructure of diphenylnitrone **2** towards substructure of (*E*)-*β*-nitrostyrenes **1a–c**. As expected, the magnitude of the charge transfer increases with the increase of electrophilicity of the substituent R in nitrostyrene. Moreover, there is a significant difference in the values of t depending on the type of the isomer formed. In general, the charge transfer is highest in the case of the formation of 4-nitroisoxazolidines **3a–c** and **4a–c** (Table 2).

The calculated activation enthalpies ($\Delta H^{\neq}_{353}$)and free enthalpies ($\Delta G^{\neq}_{353}$)indicate that in the gas phase the reactivity of (*E*)-*β*-nitrostyrenes increases with increase in electron-withdrawing character of the substituent R (**1c** > **1a** > **1b**), which is in agreement with the kinetic data obtained for these reactions in toluene solution.[9] The observed substituent effect on reactivity is consistent with the perturbation interaction diagram elaborated by us on the basis of estimated energies of the frontier molecular orbitals (FMO) for reactants **2** and **1a–c** (Fig. 3). It is evident from this diagram that the energy gaps between the HOMO of **2** and LUMO of **1a–c** (ΔE1) are smaller than those that are between the HOMO of **1a–c** and the LUMO of **2** (ΔE2). Furthermore, it is evident from Fig. 3 that ΔE1 decreases with increase in electron-

Table 2. Molecular properties from the AM1 and AM1/COSMO calculations of stationary structures for [2 + 3] cycloaddition of (*E*)-*β*-nitostyrenes **1a–c** with (*Z*)-C,N-diphenylnitrone **2**

Solvent (ε)	Reactants	Path	Structure	Bond length (Å)					Angle (°)	ΔH_{353} (kcal mol^{-1})	ΔS_{353} (cal/mol^{-1} deg^{-1})	μ(D)	t (e)	Charge (e) on the reaction sites[a]			
				O1—N2	N2—C3	C3—C4	C4—C5	C5—O1	O1—N2—O3					O1	C3	C4	C5
Gas phase	**1a**+**2**	**A—D**	**1a**+**2**	1.228	1.337	—	1.347	—	126.14	122.62	196.1	—	—	−0.445	−0.209	−0.218	−0.010
(1.0)		**A**	**LM**	1.230	1.336	6.358	1.348	3.381	126.29	118.16	135.5	7.95	0.00	−0.485	−0.170	−0.236	0.002
			TS	1.260	1.373	2.332	1.408	1.909	117.81	148.87	132.0	5.98	0.15	−0.332	0.024	−0.353	0.083
			P	1.347	1.502	1.566	1.543	1.464	108.64	103.74	128.1	3.56	—	−0.186	−0.040	−0.132	0.031
		B	**LM**	1.228	1.337	6.551	1.348	3.324	125.93	116.82	136.6	4.72	0.00	−0.481	−0.194	−0.239	0.004
			TS	1.261	1.372	2.290	1.411	1.888	118.03	144.31	131.9	4.49	0.16	−0.325	0.021	−0.346	0.080
			P	1.348	1,500	1.562	1.549	1.462	108.35	99.88	128.3	2.48	—	−0.188	−0.026	−0.129	0.039
		C	**LM**	1.226	1.339	5.355	1.346	3.436	125.99	119.79	132.6	2.58	0.00	−0.485	−0.171	0.002	−0.236
			TS	1.243	1.396	2.182	1.407	1.991	116.71	152.14	131.3	6.10	0.10	−0.288	−0.032	−0.125	−0.115
			P	1.356	1.505	1.561	1.547	1.561	108.34	102.26	131.7	4.62	—	−0.185	−0.028	−0.090	0.043
		D	**LM**	1.230	1.336	5,452	1.348	4.510	126.31	118.27	139.2	7.95	0.00	−0.456	−0.214	−0.016	−0.194
			TS	1.242	1.397	2.145	1.406	2.004	117.35	148.75	135.1	7.54	0.10	−0.283	−0.042	−0.120	−0.114
			P	1.373	1.506	1.559	1.545	1.430	107.27	99.20	136.0	6.09	—	−0.162	−0.021	−0.081	0.016
	1b+**2**	**A—D**	**1b**+**2**	1.228	1.337	—	1.349	—	126.14	130.58	213.3	—	—	−0.445	−0.209	−0.210	−0.010
		A	**LM**	1.228	1.337	7.678	1.349	5.218	125.89	127.91	151.5	8.83	0.00	−0.471	−0.190	−0.248	0.015
			TS	1.260	1.373	2.326	1.410	1.911	117.75	157.63	147.6	6.39	0.14	−0.334	0.024	−0.356	0.096
			P	1.347	1.502	1.565	1.544	1.465	108.63	112.76	146.7	4.40	—	−0.188	−0.011	−0.130	0.042
		B	**LM**	1.227	1.337	6.558	1.350	3.340	125.91	124.80	145.3	6.35	0.00	−0.477	−0.198	−0.260	0.023
			TS	1.261	1.373	2.283	1.412	1.892	117.93	153.55	150.8	5.95	0.14	−0.329	0.021	−0.346	0.094
			P	1.348	1.500	1.562	1.550	1.462	108.38	108.73	137.1	3.99	—	−0.186	−0.027	−0.130	0.050
		C	**LM**	1.224	1.339	5.262	1.348	3.533	126.03	128.08	148.5	4.81	0.00	−0.449	−0.218	0.006	−0.220
			TS	1.242	1.397	2.173	1.408	1.997	116.65	161.36	147.0	6.59	0.08	−0.282	−0.047	−0.100	−0.124
			P	1.357	1.505	1.561	1.548	1.436	108.34	111.19	144.7	5.63	—	−0.164	−0.022	−0.068	0.017
		D	**LM**	1.228	1.337	6.873	1.350	4.839	126.32	127.09	151.3	9.41	0.00	−0.471	−0.186	−0.020	−0.250
			TS	1.242	1.399	2.137	1.407	2.009	117.27	157.86	150.3	8.53	0.09	−0.289	−0.037	−0.105	−0.288
			P	1.373	1.506	1.559	1.546	1.430	107.34	107.90	148.1	7.27	—	−0.186	−0.030	−0.077	−0.042
	1c+**2**	**A—D**	**1c**+**2**	1.228	1.337	—	1.345	—	126.14	129.32	208.0	—	—	−0.445	−0.209	−0.192	−0.036
		A	**LM**	1.230	1.336	6.546	1.346	3.275	125.89	121.94	136.9	5.06	0.00	−0.495	−0.183	−0.020	−0.212
			TS	1.260	1.373	2.338	1.407	1.903	117.80	153.49	143.3	6.64	0.18	−0.328	0.030	0.064	−0.352
			P	1.328	1.502	1.567	1.543	1.462	108.58	109.18	139.8	4.79	—	−0.183	−0.008	0.021	−0.134
		B	**LM**	1.230	1.336	6.488	1.346	3.247	125.90	121.92	137.5	5.12	0.00	−0.495	−0.183	−0.020	−0.212
			TS	1.261	1.371	2.294	1.410	1.879	118.00	148.34	136.4	5.74	0.18	−0.321	0.025	0.061	−0.346
			P	1.349	1.500	1.563	1.548	1.460	108.37	104.73	133.1	4.93	—	−0.187	−0.025	0.030	−0.130
		C	**LM**	1.226	1.338	5.351	1.344	3.298	125.97	125.56	143.8	4.45	0.00	−0.466	−0.209	−0.165	−0.039
			TS	1.247	1.391	2.220	1.406	1.960	116.84	155.87	139.5	6.50	0.14	−0.282	−0.027	−0.168	−0.086
			P	1.353	1.506	1.562	1.547	1.436	108.37	106.92	136.4	4.26	—	−0.149	−0.021	−0.096	0.009
		D	**LM**	1.231	1.335	5.431	1.345	3.273	126.20	122.60	144.0	4.48	0.00	−.0497	−0.171	−0.190	−0.039
			TS	1.246	1.393	2.179	1.406	1.970	117.51	152.90	143.0	5.10	0.14	−0.285	−0.017	−0.171	−0.088
			P	1.374	1.507	1.560	1.545	1.430	107.13	104.76	137.1	4.07	—	−0.183	−0.025	−0.103	0.041
Toluene	**1a**+**2**	**A–D**	**1a**+**2**	1.231	1.336	—	1.348	—	125.73	109.43	196.5	—	—	−0.511	−0.178	−0.278	0.008
(2.4)		**A**	**LM**	1.232	1.335	4.510	1.349	5.515	125.57	108.16	135.6	5.62	0.00	−0.517	−0.185	−0.229	0.013

	TS	1.271	1.360	2.461	1.415	1.830	119.09	138.57	136.3	8.03	0.21	−0.343	0.058	−0.427	0.132
	P	1.347	1.501	1.566	1.544	1.465	108.59	95.09	134.8	4.24	—	−0.198	−0.012	−0.127	0.032
B	**LM**	1.232	1.335	6.338	1.349	3.317	125.82	106.98	131.6	5.37	0.00	−0.513	−0.176	−0.233	0.018
	TS	1.270	1.360	2.385	1.417	1.825	119.02	134.47	136.0	6.12	0.20	−0.333	0.051	−0.404	0.121
	P	1.348	1.501	1.562	1.550	1.463	108.36	91.31	132.2	2.79	—	−0.199	−0.025	−0.124	0.038
C	**LM**	1.230	1.336	5.365	1.347	3.426	125.78	109.36	133.0	3.33	0.00	−0.501	−0.192	−0.003	−0.200
	TS	1.224	1.398	2.162	1.409	1.993	116.43	142.86	127.9	7.32	0.10	−0.304	−0.030	−0.119	−0.108
	P	1.353	1.506	1.562	1.546	1.435	108.38	92.71	132.1	5.15	—	−0.164	−0.024	−0.085	0.022
D	**LM**	1.232	1.335	5.374	1.349	5.374	125.84	106.83	129.5	5.27	0.00	−0.514	−0.178	0.017	−0.233
	TS	1.244	1.400	2.121	1.409	2.000	116.97	139.33	135.4	8.87	0.09	−0.307	−0.025	−0.119	−0.109
	P	1.359	1.496	1.561	1.545	1.433	108.87	90.17	131.2	5.47	—	−0.179	−0.017	−0.091	0.037
1b+2	**A–D**	1.231	1.336	—	1.351	—	125.73	115.91	210.0	—	—	−0.511	−0.178	−0.246	0.029
A	**LM**	1.232	1.335	6.337	1.352	3.342	125.85	113.38	150.3	7.19	0.00	−0.511	−0.181	−0.259	0.037
	TS	1.270	1.361	2.438	1.416	1.837	118.87	145.85	148.0	8.00	0.20	−0.344	0.058	−0.427	0.142
	P	1.347	1.501	1.566	1.545	1.465	108.69	102.35	140.1	4.92	—	−0.200	−0.012	−0.126	0.042
B	**LM**	1.232	1.335	6.408	1.352	3.340	125.80	113.87	151.8	7.28	0.00	−0.510	−0.182	−0.250	0.038
	TS	1.270	1.362	2.368	1.418	1.830	118.80	142.16	151.3	7.59	0.19	−0.336	0.050	−0.399	0.130
	P	1.348	1.501	1.562	1.550	1.463	108.44	98.67	140.3	3.82	—	−0.199	−0.025	−0.125	0.048
C	**LM**	1.231	1.336	6.212	1.351	8.777	125.68	115.34	145.5	7.12	0.00	−0.508	−0.185	0.029	−0.247
	TS	1.244	1.399	2.153	1.410	1.999	116.36	150.72	143.4	8.94	0.08	−0.303	−0.038	−0.097	−0.118
	P	1.353	1.506	1.562	1.547	1.435	108.39	100.22	143.9	6.97	—	−0.166	−0.022	−0.074	0.022
D	**LM**	1.231	1.336	8.331	1.351	9.874	125.59	115.00	145.9	13.4	0.00	−0.513	−0.182	0.031	−0.248
	TS	1.243	1.401	2.114	1.410	2.008	116.89	146.96	144.0	10.8	0.08	−0307	−0.031	−0.105	−0.118
	P	1.373	1.506	1.559	1.545	1.430	107.47	97.10	146.7	9.02	—	−0.196	−0.031	−0.077	0.052
1c+2	**A–D**	1.231	1.336	—	1.364	—	125.73	111.76	208.7	—	—	−0.511	−0.178	−0.186	−0.019
A	**LM**	1.234	1.335	6.344	1.347	3.354	125.91	109.26	137.7	5.88	0.00	−0.527	−0.158	−0.198	−0.010
	TS	1.289	1.329	3.608	1.416	1.707	123.32	134.13	141.5	8.75	0.37	−0.361	0.089	−0.535	0.203
	I	1.316	1.327	3.523	1.451	1.529	122.17	132.94	137.9	14.0	0.66	−0.242	0.162	−0.584	0.169
	TS	1.313	1.345	2.650	1.459	1.534	120.29	135.89	129.2	12.6	0.49	−0.212	0.188	−0.564	0.128
	P	1.357	1.501	1.561	1.547	1.453	108.93	95.57	143.8	4.47	—	−0.199	−0.016	−0.113	0.033
B	**LM**	1.234	1.335	5.388	1.347	3.273	125.78	108.94	134.0	5.55	0.00	−0.522	−0.167	−0.198	−0.012
	TS	1.289	1.327	3.466	1.418	1.716	124.04	133.24	141.1	10.9	0.37	−0.351	0.090	−0.515	0.200
	I	1.316	1.326	3.513	1.454	1.540	123.15	132.40	144.9	13.4	0.72	−0.241	0.168	−0.563	0.168
	TS	1.308	1.337	2.608	1.456	1.556	121.35	133.97	135.4	11.1	0.47	−0.225	0.162	−0.545	0.135
	P	1.349	1.500	1.563	1.548	1.451	108.41	92.11	136.8	5.43	—	−0.198	−0.025	−0.125	0.028
C	**LM**	1.231	1.336	5.304	1.346	3.179	125.57	110.88	134.0	5.09	0.00	−0.503	−0.193	−0.029	−0.164
	TS	1.249	1.392	2.208	1.408	1.960	116.61	142.51	139.9	7.28	0.15	−0.304	−0.013	−0.172	−0.075
	P	1.345	1.506	1.562	1.546	1.435	108.41	93.50	136.8	4.85	—	−0.162	−0.023	−0.098	0.020
D	**LM**	1.231	1.335	5.015	1.345	3.149	125.69	111.50	141.3	5.16	0.00	−0.508	−0.188	−0.015	−0.177
	TS	1.247	1.394	2.159	1.409	1.969	117.14	139.27	136.6	5.73	0.14	−0.305	−0.009	−0.167	−0.079
	P	1.373	1.506	1.559	1.548	1.427	107.56	91.79	141.1	4.58	—	−0.182	−0.031	−0.100	0.047

[a] In the case of individual *β*-nitrostyrenes, site C4 means the *β*-carbon atom of the nitrovinyl moiety and site C5 in the *α*-carbon atom.

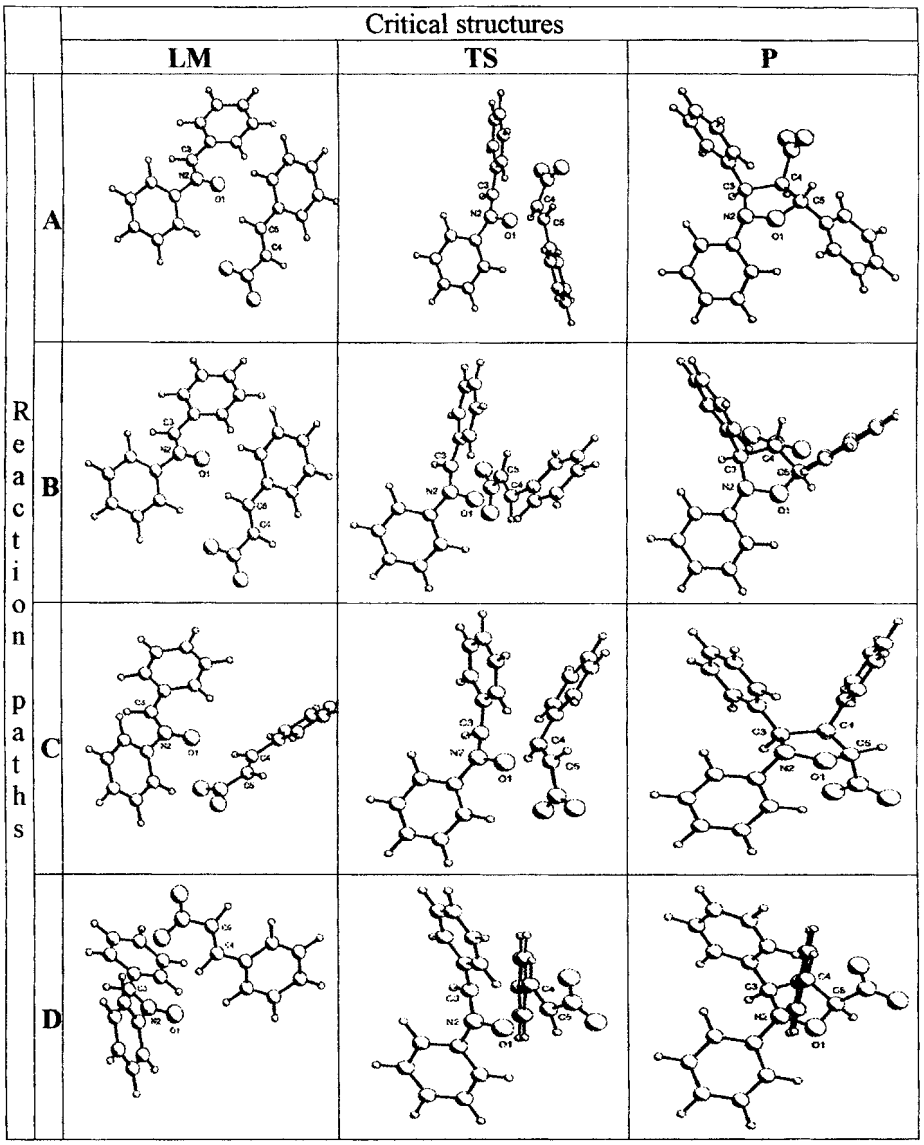

Figure 2. PLUTO views of stationary structures for [2 + 3] cycloaddition of (*E*)-*β*-nitrostyrene (**1a**) with (*Z*)-C,N-diphenylnitrone (**2**) in the gas phase

withdrawing character of substituent in *β*-nitrostyrene. Consequently, according to PMO theory,[16] the reactivity of these nitrostyrenes should increase in the same order.

Concerning the regio- and stereoselectivity of the reaction, it is evident that the formation of nitroisoxazolidines according to path **B** is favored (Table 3). The highest activation barrier occurs on path **C**. The activation parameters for paths **A** and **D** are located in between, while the former path shows higher activation enthalpy than the latter. If the interaction diagram is used for predicting the reaction regioselectivity, then according to the PMO theory,[16] the interaction of both pairs of FMO favors formation of 4-nitroisoxazolidines **3a**–**c** and **4a**–**c**. The discrepancy between the results obtained on the basis of PMO theory and those obtained directly from PES calculation seems to prove a notable effect of steric factors on the reaction regioselectivity (at least within the gas phase).

In general, the magnitude of the activation enthalpies suggests that the rehybridization of the reaction sites in the studied transition states is not highly evolved. On the other hand, the large negative values of the activation entropy indicate a high ordering of reactants in the reaction system. These are characteristic features of a concerted reaction mechanism. However, evaluation of the full meaning of the calculated Eyring parameters is not easy, because the kinetics of the reactions studied have not been an object of experimental investigations in the gas phase.

The AM1/COSMO calculations for the [2 + 3] cycloaddition of nitrostyrenes **1a** and **1b** to diphenylnitrone **2** in toluene solution predict, as in the gas phase

Table 3. Relative thermodynamic parameters[a] of stationary structures calculated for the [2 + 3] cycloaddition of (*E*)-*β*-nitrostyrenes **1a–c** to diphenylnitrone **2** (reference: sum of the values of suitable thermodynamic parameters calculated for the reactants, $T = 353$ K)

Solvent (ε)	Reactants	Stationary structure	Path **A**			Path **B**			Path **C**			Path **D**		
			$\Delta H^{\neq}$	$\Delta S^{\neq}$	$\Delta G^{\neq}$	$\Delta H^{\neq}$	$\Delta S^{\neq}$	$\Delta G^{\neq}$	$\Delta H^{\neq}$	$\Delta S^{\neq}$	$\Delta G^{\neq}$	$\Delta H^{\neq}$	$\Delta S^{\neq}$	$\Delta G^{\neq}$
Gas phase (1.0)	**1a**+**2**	**LM**	−4.46	−60.6	16.93	−5.80	−59.5	15.20	−2.83	−63.5	19.59	−4.35	−56.9	15.74
		TS	26.25	−64.1	48.88	21.69	−64.2	44.35	29.52	−64.8	52.39	25.73	−61.0	47.26
		P	−18.88	−68.0	5.12	−22.74	−67.8	1.19	−19.76	−64.4	2.97	−23.42	−60.1	−2.20
	1b+**2**	**LM**	−2.67	−61.8	19.15	−5.78	−68.0	18.22	−2.50	−64.8	20.37	−3.49	−62.0	18.96
		TS	27.05	−65.7	50.24	22.97	−62.5	45.03	39.78	−66.3	54.18	27.28	−63.0	49.51
		P	−17.82	−67.3	5.93	−21.85	−76.2	5.05	−18.68	−68.6	5.53	−22.68	−65.2	0.34
	1c+**2**	**LM**	−7.38	−71.1	17.72	−7.40	−70.5	17.49	−3.76	−64.2	18.90	−6.72	−64.0	15.87
		TS	24.17	−64.7	47.01	19.02	−71.6	44.29	26.55	−68.5	50.73	23.58	−65.0	46.53
		P	−20.14	−68.8	4.15	−24.59	−74.9	1.85	−22.40	−71.6	2.87	−24.56	−70.9	0.47
Toluene (ε)	**1a**+**2**	**LM**	−1.27	−60.9	20.22	−2.45	−64.9	20.46	−0.07	−63.5	22.35	−2.60	−67.0	21.05
		TS	29.14	−60.2	50.39	25.04	−60.5	46.40	33.43	−68.6	57.65	29.90	−61.1	51.47
		P	−14.34	−61.7	7.44	−18.12	−64.3	4.58	−16.72	−60.4	4.60	−19.13	−65.3	3.92
	1b+**2**	**LM**	−2.53	−59.7	18.54	−2.04	−58.2	18.50	−0.57	−64.5	22.20	−0.91	−64.1	21.71
		TS	29.94	−62.0	51.83	26.25	−58.7	46.97	34.81	−66.6	58.31	31.05	−66.0	54.35
		P	−13.56	−69.9	11.11	−17.24	−69.7	7.36	−15.69	−66.1	7.64	−18.81	−63.3	3.53
	1c+**2**	**LM**	−2.50	−71.0	22.56	−2.82	−74.7	23.55	−0.88	−74.7	25.48	−0.26	−67.4	23.53
		TS	22.37	−67.2	46.09	21.48	−67.2	45.20	—	—	—	—	—	—
		I	21.18	−70.8	46.17	20.64	−63.8	43.16	—	—	—	—	—	—
		TS	24.13	−79.5	52.19	22.21	−73.3	48.08	30.75	−68.8	55.04	27.51	−72.1	52.96
		P	−16.19	−64.9	6.72	−19.65	−71.9	5.73	−18.26	−71.9	7.12	−19.97	−67.6	3.89

[a] $\Delta G^{\neq}$ *and* $\Delta H^{\neq}$ in kcal mol^{-1} and $\Delta S^{\neq}$ in cal mol^{-1} K^{-1}.

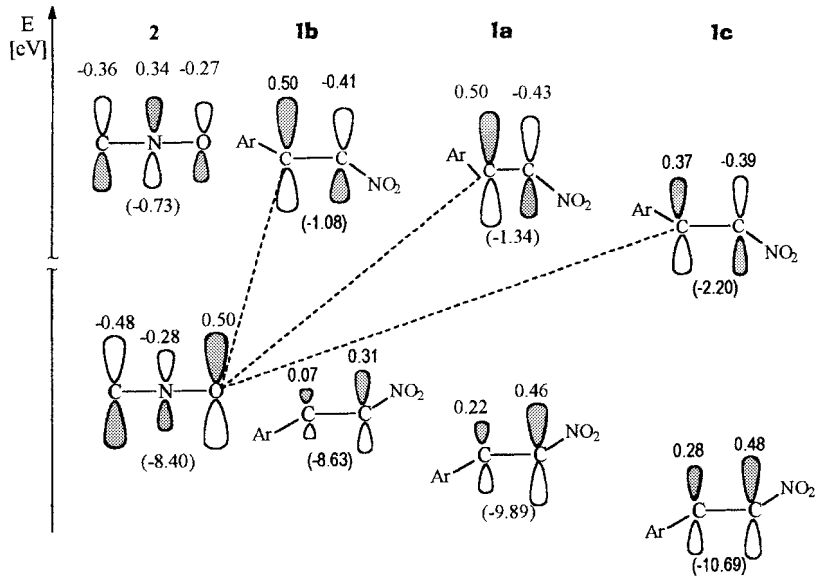

Figure 3. Correlation diagram for the [2 + 3] cycloaddition of (*E*)-*β*-nitrostyrenes **1a**–**c** to (*Z*)-C,N-diphenylnitrone **2**. Data for plot taken from AM1 calculations; energies of HOMO and LUMO are given in parentheses

(Fig. 1), only **LM** and **TS** structures between the structures of **R** and **P** along each studied reaction pathway. Their geometric dimensions are similar to those found for the gas phase, but other physical properties are slightly changed (Table 2). In particular, all local minima are shallower and their enthalpy of formation from the substrates does not exceed -2.6 kcal mol^{-1}. Moreover, the large negative entropy of formation of these causes, as a rule, the corresponding $\Delta G^{\neq}_{353}$to be higher than the $\Delta G^{\neq}_{353}$calculated for the gas phase. One has to keep in mind, however, that entropy value calculated by the COSMO procedure can be impaired by a relatively large error [13,14].

The **TS** structures also changed slightly but solely in the case of paths **C** and **D**. For paths **A** and **B** asymmetry of the transition states increased significantly. The differences in the lengths of the newly formed *σ*-bonds increased up to ca 0.6 Å. These changes, when combined with the ca 30% increase in *t*, suggest that increasing the alkene electrophilicity should favor the reaction course according to a zwitterionic mechanism.[17,18]

Actually, when nitrostyrene **1c** was involved in calculations as dipolarophile, between structures **R** and **P** four stationary structures were found on paths **A** and **B** (Figs 4 and 5, Table 2). Initially, as in the gas phase, interaction of **1c** with **2** leads with any activation barrier to supermolecules **LM**, which are similar to those obtained for the other two pairs of reactants. Each of them contains a practically undistorted structure of dinitrostyrene **1c** and diphenylnitrone **2** at a distance that is outside the characteristic range for covalent bonding. As the reactants approach each other, structures **TS′** appears on paths **A** and **B**. Analysis of the Hessian matrices revealed that in both cases there was only one negative force constant in each matrix, corresponding to imaginary frequencies of 392.9i and 379.4i cm^{-1}, respectively. Both **TS′** structures are extremely unsymmetrical. In the case of path **A** the C3—C4 and C5—O1 distances are 3.608 and 1.707 Å, whereas for path **B** they are 1.466 and 1.716 Å. As can be seen for each path, the latter distance is characteristic of the transition state, while the former is far beyond the range of distances characteristic of the saddle point in the gas phase (cf. data in Table 2).

Movement forward along both reaction paths leads to structures of intermediates **I**. The Hessian matrices calculated for structures **I** did not show any negative eigenvalue. Their energy is higher than that of the reactants **R** and also the final products **P** (Fig. 4, Table 3). Both structures already have a fully formed C5—O1

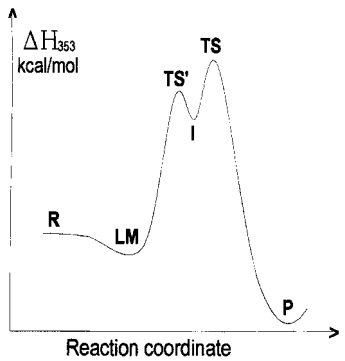

Figure 4. Typical reaction profile for the [2 + 3] cycloaddition of *p*,*β*-dinitrostyrene (**1c**) to (**Z**)-C,N-diphenylnitrone (**2**) in toluene solution according to paths **A** and **B**. Structures at the marked points are depicted in Fig. 5

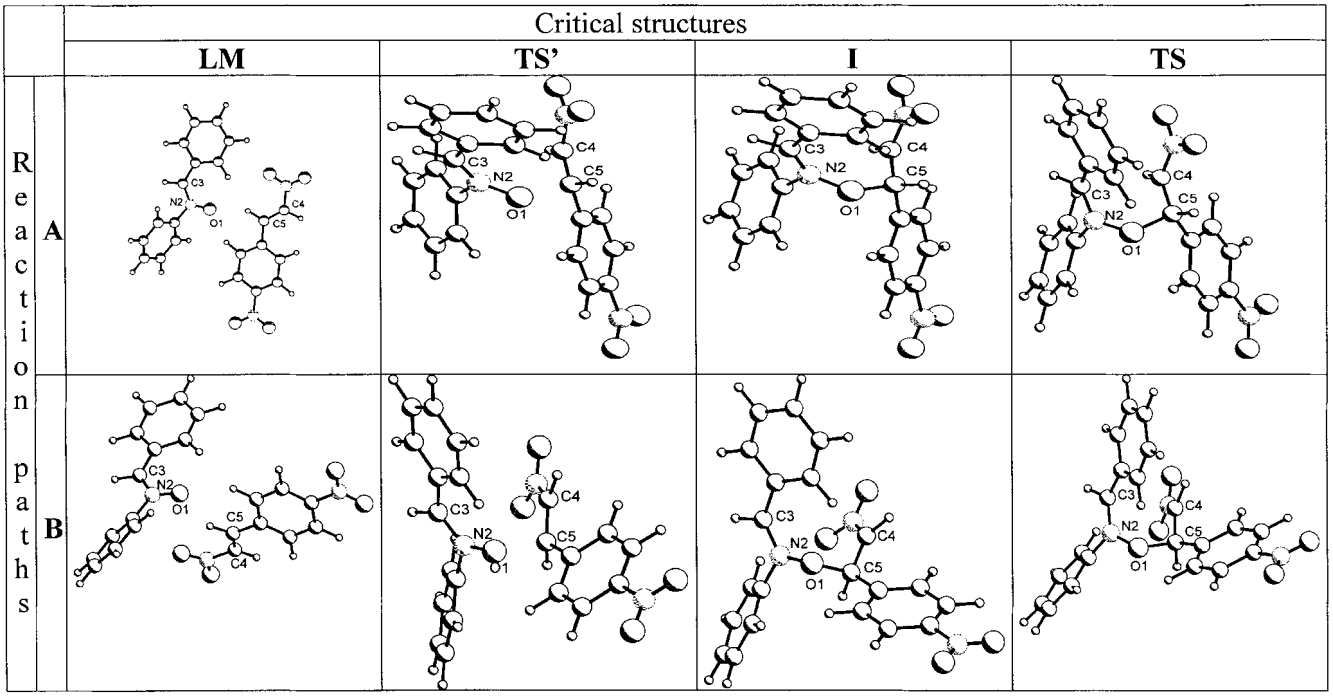

Figure 5. PLUTO views of stationary structures for [2 + 3] cycloaddition of *E*-p,*β*-dinitrostyrene (**1c**) with *Z*-C,N-diphenylnitrone (**2**) in toluene solution according to paths **A** and **B**

bond (Fig. 5) of length 1.529 and 1.540 Å, respectively; however, the other key distances still remain very large and equal 3.523 and 3.513 Å, respectively. Moreover, there is a very large charge separation in these structures. According to Mulliken population analysis, 0.66*e* is transferred to the substructure of dinitrostyrene from that of diphenylnitrone in **I** on path **A**, and 0.72 *e* in **I** on path **B**. Therefore, it seems that both intermediates should be interpreted in terms of a zwitterion.

As the reaction progresses, the distance between the center C4 and C3 decreases, and the transition states **TS** appear on the PES. Analogously as in the case of transition states **TS′**, the analysis of the Hessian matrix showed a single negative eigenvalue, corresponding to imaginary frequencies of 202.7i and 110.6i cm^{-1}, respectively, in the case of paths **A** and **B**. The calculated transition vectors connect minima of intermediates **I** with the minima of the corresponding cycloadducts **P**, which confirms that these stationary points are true transition states for the conversion of **I** into **P**. The structures of both **TS** are not symmetric, but the lengths of the newly formed bonds are within the range of distances characteristic of transition states calculated for the cycloaddition of other studied reactants (Table 2). In both cases the charge transfer takes place in the direction from substructure of 1,3-dipole to substructure of dipolarophile, but it is substantially smaller than in intermediates **I**, but larger than in transition states **TS′**. The enthalpy change of the first stage of the reaction (**R**→**I**) along path **B** is 0.89 kcal mol^{-1} lower than that along path **A**. For the second stage (**I**→**P**) the trend is the same; the enthalpy change along path **B** is 1.38 kcal mol^{-1} lower than that along path **A**.

For the reaction of **1c** and **2** along paths **C** and **D**, analogously as in gas phase (Fig. 1), between **R** and **P** only two critical structures, namely **LM** and **TS**, were localized. Their molecular properties were similar to those obtained for other studied reactants (Table 2).

The activation parameters calculated for the reaction of **1a–c** with **2** in toluene solution are collected in Table 3. They indicate a variation of the activation enthalpy from 34.81 to 22.21 kcal mol^{-1}, and of the activation entropy from −79.5 to −60.2 cal mol^{-1} K^{-1} depending on the reaction path and dipolarophile used. It should be noted that the activation parameters for several nitrone cycloadditions on to *para*-substituted *β*-nitrostyrenes in toluene solution have been measured in our laboratory. It was found that these reactions are characterized by modest activation enthalpies ranging between 16 and 17 kcal mol^{-1}, and negative entropies of activation, ranging from 28 to 32 cal mol^{-1} K^{-1}. Hence the AM1/COSMO values are considerably overestimated. Nevertheless, they indicate that, in toluene solution, the reactions along paths **B** and **A** should be fastest, while path **B** should still be preferred. The reactivity order of nitrostyrenes **1a–c** in comparison with the gas phase remains unchanged. These results are in good agreement with the PMO predictions (Fig. 3) and with the experimental data.[8,9]

In toluene solution the activation barriers are, as a rule,

higher than those calculated for the gas phase, which suggests that the reaction should slow with an increase in the polarity of the medium. This suggestion, although requiring additional calculations, is in agreement with our recent kinetic study performed for the reaction of **1a** with **2** in reaction media with different ionizing powers.[8]

CONCLUSIONS

The AM1 calculations carried out for the gas phase suggest a concerted reaction mechanism for the [2 + 3] cycloaddition of (*E*)-*β*-nitrostyrenes **1a**–**c** with (*Z*)-C,N-diphenylnitrone **2**. While the formation of 2,3-diphenyl-4-aryl-5-nitroisoxazolidines (paths **C** and **D**) seems to occur almost synchronously, in the case of 2,3-diphenyl-5-aryl-4-nitroisoxazolidines (paths **A** and **B**) there is considerably transition state asymmetry. The activation barriers obtained indicate that the reaction paths **B** and **D** are favored. The highest activation barrier occurs on path **C**. This trend changes in toluene solution, as shown by the AM1/COSMO calculations. In the latter case, the reaction paths can be ordered in the sequence **B** >**A** >**D** >**C**. An increase in the polarity of the reaction medium causes elevation of the particular activation barriers and in some cases changes the reaction mechanism. An increase in the electron-withdrawing character of the substituent in the benzene ring of (*E*)-*β*-nitrostyrene speeds up the reaction both in the gas phase and in toluene solution but does not affect the reaction regio- and stereoselectivity. It should be noted, however, that the solvent effect calculated from the COSMO procedure does not account for specific effects such as charge transfer and polarizability phenomena, which may be important with the activated aromatic systems of solutes and solvent.[14,24]

Acknowledgements

The generous allocation of computer time by the regional computer center CYFRONET in Kracow and financial support by the Polish Committee of Scientific Research (Grant No. KBN/SPP/PK/076) is gratefully acknowledged.

REFERENCES

1. Baranski A. *J. Mol. Struct. (Theochem)* 1998; **432**: 229.
2. Baranski A. *J. Mol. Struct. (Theochem)* 1999; **499**: 185.
3. Baranski A, Taborski W. *Khim. Khim. Tekhnol.* 1999; **42**: 17.
4. Frederickson M. *Tetrahedron* 1997; **53**: 403.
5. Tuffariello JJ. In *1,3-Dipolar Cycloaddition Chemistry*, vol. 2, Padwa A (ed). John Wiley and Sons; New York, 1984; Chapt. 9.
6. Grunanger P, Vita-Finzi P. In *The Chemistry of Heterocyclic Compound*, vol. 49, Taylor EC (ed). Wiley–Interscience: New York, 1991; Chapt. 3.
7. Joucla M, Gree D, Hamelin J. *Tetrahedron* 1973; **29**: 2315.
8. Baranski A. *Poli. J. Chem.* 1999; **73**: 1711.
9. Taborski W, Baranski A. In Abstracts of Papers of VII International Conference on the Problems of Solvatation and Complex Formation in Solutions, June 29–July 2, 1998, Ivanovo (Russia). 1998; 367.
10. Bayer JH. In *Nitroazoles*, Feuer H (ed). VCH: Deerfield Beach, FL, 1986.
11. Baranski A, Kelarev VI. *Chem. Heterocyl. Compd. (Engli. Transl.)* 1990; 371.
12. Pascal YL, Chanet-Ray J, Vessiere R, Zeroual A. *Tetrahedron* 1992; **48**: 7197.
13. Stewart JJJ. *MOPAC 93 Manual*, Fujitsu: Tokyo, 1993.
14. Klamt A, Shüürmann G. *J. Chem. Soc., Perkin Trans. 2* 1993; 799.
15. Leroy G, Sana M, Burke LA, Nguyen MT. *Quantum Theory Chem. React.* 1980; **1**: 91.
16. Klopman G. In *Chemical Reactivity and Reaction Paths*, Klopman G (ed). John Wiley & Sons: New York, 1974.
17. Huisgen R, Langhals E, Mloston G, Oshima T, Rapp J. *J. Heterocycli Chem. (Suppl. Issue)*, 1987; **24**: S-1.
18. Huisgen R. In *1,3-Dipolar Cycloaddition Chemistry*, vol. 1, Padwa A (ed). John Wiley & Sons: New York, 1984; Chapt. 1.
19. Cioslowski J, Baranski A, Juska T. *Tetrahedron* 1986; **42**: 4549.
20. Vasil'eva VN, Perekalin VV, Vasil'ev VG. *Zh. Obshch. Khim.* 1961; **31**: 2171.
21. Samuilov YaD, Solovieva SE, Konovalov AI. *Zh. Org. Khim.* 1980; **16**: 1228.
22. Baliah V, Chandrasekharan V. *Indian J. Chem.* 1970; **8**: 1096.
23. Gothelf KV, Hazell RG, Jorgensen KA. *Acta Chem. Scand.* 1997; **51**: 1234.
24. Klamt A. *J. Phys. Chem.* 1995; **22**: 2224.